ARTICLE

Exploiting the interaction between halloysite and charged PNAs for their controlled release

\Received 00th January 20xx,
Accepted 00th January 20xx

DOI: 10.1039/x0xx00000x

Serena Riela,[a] Raquel de Melo Barbosa,[b] Ana Borrego-Sánchez,[c] Silvia Cauteruccio,[d,*] Marina Massaro,[a,*] C. Ignacio Sainz-Díaz,[e] Rita Sánchez-Espejo[b], César Viseras-Iborra,[b,e] and Emanuela Licandro[d]

The design and development of nanomaterials that could be used in nanomedicine is of fundamental importance to obtain smart nanosystems for the treatment of several diseases. Halloysite, because of its interesting features, represents a suitable nanomaterial for the delivery of different biologically active species. Among them, peptide nucleic acids (PNAs) have attracted considerable attention in recent decades for their potential applications in both molecular antisense diagnosis and as therapeutic agents, although up to now, the actual clinical applications are very limited. Herein we report a systematic study on the supramolecular interaction of three differently charged PNAs with halloysite. Understanding the interaction mode of charged molecules with the clay surfaces represents a key factor for the future design and development of halloysite based materials which could be used for the delivery and subsequent intracellular release of PNA molecules. Thus, three different PNA tetramers, chosen as models, were synthetized and loaded onto the clay. The obtained nanomaterials were characterized by spectroscopic studies, thermogravimetric analysis and their morphologies were studied by high angle annular dark field transmission electron microscopy (HAADF/STEM) coupled with Energy Dispersive X-ray spectroscopy (EDX). The aqueous mobility of the three different nanomaterials was investigated by dynamic light scattering (DLS) and ζ-potential measurements. The release of PNA tetramers from the nanomaterials was investigated at two different pH, mimicking physiological conditions. Finally, to better understand the stability of the PNA synthetized and their interactions with HNTs, molecular modelling calculations were also performed. The obtained results showed that PNA tetramers interact in different way with HNTs surfaces according to their charge which influences their kinetic release in media mimicking the phisiological conditions.

Introduction

Nanotechnology is developing rapidly in various fields, seeking natural or synthetic materials that can be easily adhered on a large scale and at low cost. The morphology of such nanomaterials appears as fibrous[1] or consisting of sheets with tubular structures that are based on different compositions, such as carbon, or phyllosilicates-based materials. The particular structure of nanomaterials, indeed, has provided outstanding advantages because of their unique properties such as the nanoscale size, high surface area, and tunable surface chemistry. In this context, clay minerals, phyllosilicates having nanometric dimensions used in healthcare since ancient times due to their intrinsic properties, are ones of the most promising.[2, 3]

Halloysite is an aluminosilicate clay, belonging to the kaolin group, which has attracted considerable attention for application in biology because of its interesting features.[4] Halloysite, with a chemical formula of $Al_2Si_2O_5(OH)_4 \times nH_2O$ is a natural and low-cost material that possesses a predominantly hollow tubular structure. Due to this feature, it is commonly known as halloysite nanotubes (HNTs). Structurally, HNTs are constituted by an external surface composed of siloxane (Si–O–Si) groups, an internal surface, a lumen, that consists of a gibbsite-like array of aluminol (Al–OH) groups, and the presence of some Al–OH and Si–OH groups at the edges of the material or as structural defects at external surface. Furthermore, ζ-potential measurements have shown that HNTs are ionized in a wide pH range, presenting a negative charge at the external surface and a positively charged lumen.

The different chemical composition at the inner and outer surfaces allows the chemical modification of the nanotubes by grafting suitable functional groups which have allowed the synthesis of different nanomaterials with hierarchical structures.[5] In addition, the opposite charges at surfaces were exploited for the immobilization, by electrostatic attraction interactions, of different molecules to obtain innovative nanomaterials for different purposes.[6, 7] In this context,

[a] Department of Biological, Chemical and Pharmaceutical Sciences and Technologies, University of Palermo Viale delle Scienze, Ed. 17 90128 Palermo, Italy. E-mail: marina.massaro@unipa.it
[b] Department of Pharmacy and Pharmaceutical Technology, Faculty of Pharmacy, University of Granada, Campus of Cartuja, 18071 s/n, Granada, Spain.
[c] Instituto de Ciencia Molecular, Universitat de València, Carrer del Catedrátic José Beltrán Martinez 2, 46980 Paterna, Spain.
[d] Department of Chemistry, University of Milan, via Golgi 19 20133 Milan, Italy- E-mail: silvia.cauteruccio@unimi.it
[e] Andalusian Institute of Earth Sciences, CSIC-UGR, Avenida de las Palmeras 4, 18100, Armilla, Granada, Spain.
Electronic Supplementary Information (ESI) available: [details of any supplementary information available should be included here]. See DOI: 10.1039/x0xx00000x

proteins or enzymes were selectively immobilized at the external surface or loaded into the lumen by working in pH ranges above or below their isoelectric points.[8] In this way, efficient nanocontainers for drug delivery or biomimetic nanoreactors were successfully synthetized.

HNTs, conversely to other tubular nanomaterials present suitable dimensions for macrophage removal. Different studies assessed the biocompatibility of HNTs[9, 10] and established that they exert relevant toxicity *in vitro* at the concentration of 1000 μg/mL;[11] whereas *in vivo* experiments highlighted that the oral administration limit is at ca. 20 mg /kg BW.[11] They also possess the intrinsic capacity to cross cellular membranes localizing in the perinuclear region.[12, 13]

Peptide nucleic acids (PNAs) can be considered one of the most powerful analogues of natural oligonucleotides and have attracted considerable attention in recent decades for their potential applications in both molecular antisense diagnosis and as therapeutic agents. Compared with natural oligonucleotides, they offer some advantages such as greater biological stability against nuclease and protease enzymes, higher specificity, and stability in interactions with complementary RNA or DNA. This is due to their chemical structure, completely different compared to that of natural nucleic acids, made of a backbone of electrostatically neutral *N*-(2-aminoethyl)glycine on which nucleobases are appended through amide bonds (Figure 1).[14] However, despite the remarkable potentialities possessed by PNAs, their poor water solubility, low uptake by eukaryotic cells, and rapid renal clearance, have so far prevented, the application of PNAs in the biomedical field. To overcome these limitations several strategies have been considered[15] even though the cellular uptake remains an unsolved issue and there are currently no drugs available based on PNA, even though a recent publication mentions one PNA drug in clinical trials, and others in development.[16]

Recently, some of us reported the covalent linkage of PNA tetramers, chosen as model, to HNTs to develop nanomaterials for intracellular PNA delivery.[17] The characterization of the obtained nanomaterial highlighted that the PNA tetramer retains its capability to bind complementary single-stranded DNA when immobilized onto HNTs.

To the best of our knowledge, to date no reports are present in literature dealing with the supramolecular loading of PNA molecules onto halloysite. This approach, being simpler than the covalent one, could represent a promising strategy for the delivery of PNA based drugs.

Herein we report a systematic study on the supramolecular interaction of three different PNAs with HNTs. Understanding the interaction mode of charged molecules with HNTs surfaces represents a key factor for the future design and scale up of the synthesis of HNTs based materials which can be used for the delivery and subsequent intracellular release of PNA molecules. Therefore, a model PNA tetramer, containing the four nucleobases A, C, G, T, was selected for this study, and three differently charged derivatives of this PNA tetramer were prepared: the positively charged PNA **1**, the negatively charged PNA **2** and the neutral PNA **3** (Figure 2).

After the PNA tetramers synthesis, they were loaded onto HNTs and the obtained nanomaterials were investigated by spectroscopic characterizations, thermogravimetric analysis and their morphologies were studied by high angle annular dark field transmission electron microscopy (HAADF/STEM) coupled with Energy Dispersive X-ray spectroscopy (EDX). The aqueous mobility of the three different nanomaterials was investigated by dynamic light scattering (DLS) and ζ-potential measurements. The release of PNA tetramers from the nanomaterials was investigated at two different pH, mimicking physiological conditions.

Lastly, computational calculations were also carried out in order to better understand and analyze the stability of the PNA synthetized and their interactions with HNTs.

Results and Discussion

The preparation of the different HNTs-PNA nanomaterials was accomplished in a two-step procedure: *i*) synthesis of the three PNA tetramers **1**–**3** endowed with appropriate terminal groups, *ii*) conjugation of PNA **1**–**3** on HNTs by exploiting the electrostatic interactions between PNAs and HNTs.

Synthesis of PNA tetramers 1–3

The PNA tetramers **1**–**3** were prepared manually according to standard protocols for solid-phase synthesis of PNAs.[18] More in detail, the positively charged PNA **1** was synthesized through two different procedures, namely the Boc/Z and Fmoc/Bhoc strategies, involving the use of the commercially available MBHA and the ChemMatrix® resins, respectively, and the properly protected PNA monomers. The MBHA resin supported PNA tetramer **4** was subjected to cleavage by stirring it in the presence of a mixture of TFA/TFMSA/*m*-cresol/thioanisole for1.5 h.

Otherwise, the ChemMatrix® resin supported PNA tetramer **5** was treated with a solution of piperidine in NMP to remove the Fmoc protecting group, then with a mixture of TFA/*m*-cresol for 1.5 h (Scheme 1).

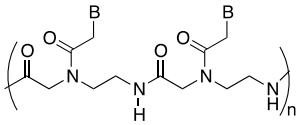

Figure 1. General structure of a portion of the polyamide backbone of peptide nucleic acid: a dimer.

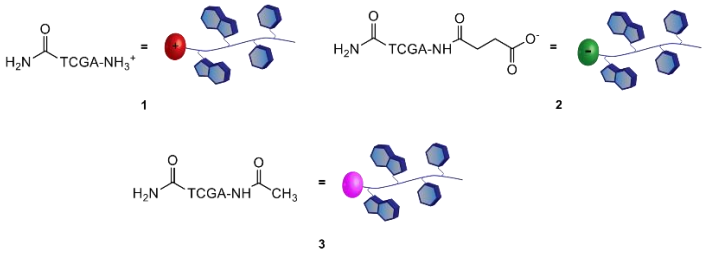

Figure 2. Structure of PNA tetramers **1**–**3**.

Both procedures provided the crude tetramer **1** that was purified by means of the RP-HPLC and analyzed by UPLC-HR-ESI$^+$ mass analysis (see Supporting Information). The resin supported PNA **4** was used as starting building block to obtain the negatively charged tetramer **2** and the neutral tetramer **3**, which were synthesized through a three-step protocol, that involved the removal of the Boc group from **4** under acidic conditions followed by the neutralization with DIPEA and the coupling with a large molar excess of succinic anhydride and acetic anhydride, to give **2** and **3** respectively (Scheme 2). After the cleavage, the crude PNA tetramers **2** and **3** were purified by RP-HPLC and analyzed by UPLC-HR-MS analysis (see Supporting Information). Both tetramers **2** and **3** were also prepared starting from resin supported PNA tetramer **5** according to Fmoc/Bhoc strategy, obtaining similar results.

Synthesis of HNTs/PNA nanomaterials

The loading of the three different PNA tetramers **1**–**3** onto halloysite was carried out by following a standard procedure adopted for the supramolecular loading of organic molecules onto HNTs.[19] In details, a dispersion of halloysite (50 mg) in water (2.5 mL) was mixed with a solution of the PNA tetramers in water (10 mM, 0.5 mL). Afterward, the dispersions were evacuated for 30 min (200 torr) and left to stir at room pressure for 15 min, and this cycle was repeated twice. Finally, the dispersions were stirred at room temperature for ca. 16 h. After work-up, the amount of PNA tetramers loaded on HNTs was of ca. 5 wt%, 6.3 wt% and 5.8 wt% for HNTs-**1**, HNTs-**2** and HNTs-**3**, respectively, as estimated by TGA. Based on the electrostatic interactions which can occur between HNTs and the three PNA tetramers, three different nanomaterials can be obtained where the PNA molecules are loaded inside the HNTs lumen (HNTs-**2**), on the external surface (HNTs-**1**) and on both surfaces (HNTs-**3**), respectively (Scheme 3).

The HNTs/PNA nanomaterials were characterized by FT-IR spectroscopy and TGA, and the colloidal properties were estimated by DLS and ζ-potential measurements. Furthermore, the morphology of the nanomaterials was imaged by TEM and high-angle annular dark field scanning transmission electron microscopy (HAADF-STEM) coupled with an EDX probe.

Firstly, the nanomaterials were characterized by thermogravimetric analysis/derivative thermogravimetry (TGA/DTG) under air atmosphere.

PNA molecules **1**–**3** totally decompose in a multi-step process occurring in a temperature range between 200 and 600 °C (Figure 3a).

On the contrary, HNTs exhibits relatively good stability up to *ca* 450 °C, then between 450 and 600 °C a mass loss occurs, due to the expulsion of the interlayer water molecules of HNTs (black line in Figure 3b). By the comparison of the TGA curves (Figure 3b) of pristine HNTs with those of HNTs/**1**, HNTs/**2** and HNTs/**3** nanomaterials, it is possible to observe that in all cases investigated, the nanomaterials, according to the presence of organic molecules, start to be degraded earlier than the pristine HNTs. Analysis of the DTG curves showed, indeed, that the HNTs/PNA nanomaterials degradation starts at ca. 240 °C, reaching stability up to 800 °C. The amount of PNA tetramers loaded into HNTs was calculated by using the rule of mixture by considering the mass losses at 25–150 °C (ML_{150}) and the residual masses at 800 °C (MR_{800}) for the pristine components (HNTs and PNA tetramers) and the HNTs/PNA nanomaterials.[20, 21] From these data it was possible to calculate the loading efficiencies reported above.

The FT-IR spectra of pristine HNTs, HNTs/**1**, HNTs/**2** and HNTs/**3** nanomaterials are reported in Figure 4. As it is possible to observe, beside the typical vibration bands of halloysite, all nanomaterials present some additional vibration features attributable to the PNA tetramers supramolecularly interacting. In detail, it is possible to observe the stretching vibration of the amide bond at ca. 1650 cm^{-1} and the peaks in the range 1600–1350 cm^{-1} related to the stretching of C=C, and C-N groups. In addition, the bands at ca. 1583, 1508, 1440, 1414 and 1290 cm^{-1} related to the stretching vibrations of the carbonyl and aromatic groups of the tetramers are also observable.

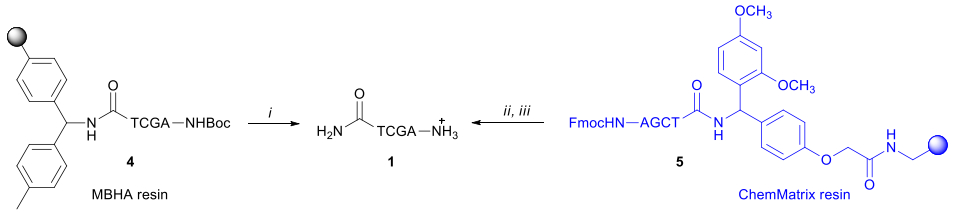

Scheme 1. Cleavage of the positively charged PNA **1**: *i*) TFA/TFMSA/*m*-cresol/thioanisole (6:2:1:1, v/v/v/v), 1.5 h; *ii*) piperidine in NMP (1:5 v/v); *iii*) TFA/*m*-cresol (9:1, v/v), 1.5 h.

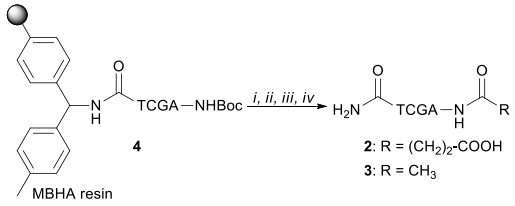

Scheme 2. Synthesis of PNA **2** and **3**: *i*) TFA/*m*-cresol (95:5); *ii*) DIPEA (5% in DCM); *iii*) succinic anhydride (20 equiv. for **2**) or acetic anhydride (20 equiv for **3**), NMP, 4 h; *iv*) TFA/TFMSA/*m*-cresol/thioanisole (6:2:1:1), 1 h.

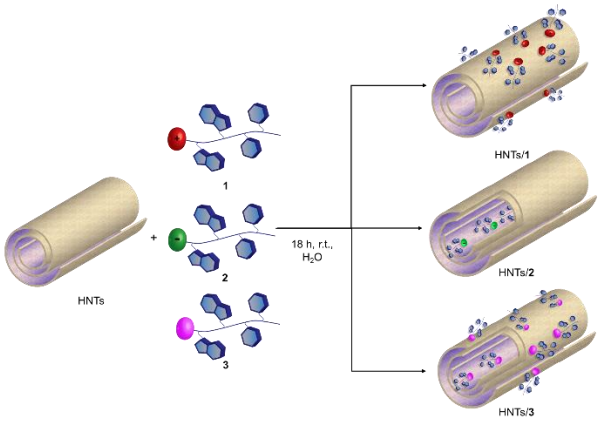

Scheme 3. Schematic representation of PNA tetramers **1**, **2** and **3** onto HNTs.

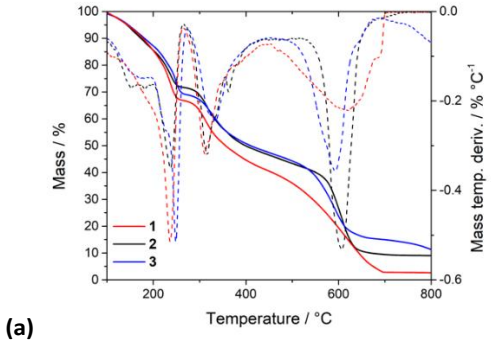

(a)

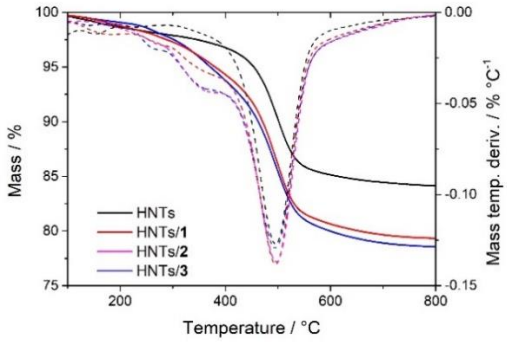

(b)

Figure 3. Thermoanalytical curves and their derivatives of (a) PNA tetramers **1**, **2** and **3**; (b) HNTs/**1**, HNTs/**2** and HNTs/**3** nanomaterials.

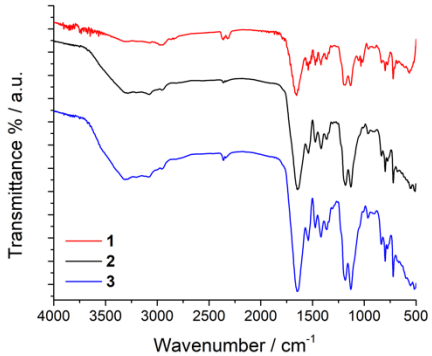

(a)

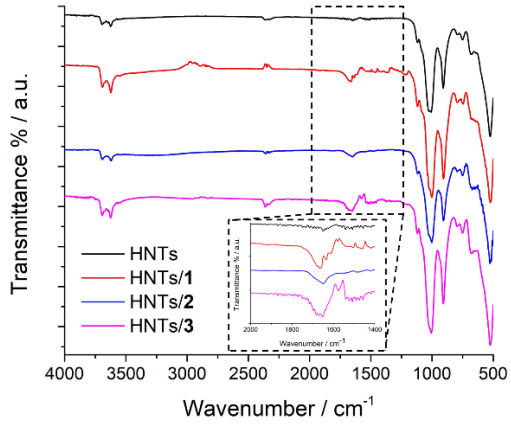

(b)

Figure 4. FT-IR spectra of (a) PNA tetramers **1**, **2** and **3**; (b) HNTs, HNTs/**1**, HNTs/**2** and HNTs/**3** nanomaterials.

The colloidal properties of the obtained HNTs nanomaterials were estimated by DLS and ζ-potential measurements. DLS measurements allow to determine structural characteristics of the nanomaterials by monitoring their mobility in water, by measuring the average translational diffusion coefficient. This coefficient considers the dimension, shape and hydration of the diffusing particles and also the existence of aggregation phenomena. By applying the Stokes-Einstein equation it is possible to calculate the average diameter of the equivalent sphere, which can be considered as an index to follow the changes in particle dimensions and interparticle aggregation. The results obtained are reported in Table 1 and Figure 5. As it is possible to note pristine HNTs showed an average size of ca. 422 nm with a polydispersity index (PDI) of ca. 0.31. Since the PDI is a measure of the heterogeneity of a certain sample based on its size, it is possible to conclude that in this case the value obtained indicates a broad size distribution of diffusing objects. After loading of positively charged PNA onto HNTs the Z-average size of the nanomaterial HNTs/**1** decreases in according to the introduction of hydrophilic moiety onto HNTs, which allows a better diffusion in aqueous medium. The HNTs/**2** nanomaterial showed a Z-average size value very similar to that of pristine HNTs, further confirming the loading in the lumen. The interaction of the clay with the uncharged PNA tetramer **3**, led to the formation of nanoparticles in dispersion which possess a Z-average size smaller than that of HNTs, this finding led us to hypothesize that the loading of **3** could occur both in the lumen and on the HNTs external surface (see *infra*). Therefore, based on these findings, it is possible to conclude that the introduction of PNA tetramers onto HNTs surfaces did not induce relevant variation in the diffusion mode of pristine HNTs so, it could be expected, for future biological applications that the HNTs/PNA nanomaterials show the same cellular uptake of halloysite.[7]

The effect of the different PNA loading onto HNTs was investigated by ζ-potential measurements in water and the obtained resulted are reported in Table 1. As it is possible to observe, all nanomaterials present a negative ζ-potential value. The nanomaterials HNTs/**1** and HNTs/**3** showed ζ-potential values closed to the one of pristine HNTs. The slight increase in

their values in comparison to HNTs further confirm the presence of PNA tetramers on the external surface. The HNTs/**2** nanomaterial presents a ζ-potential value of ca. –39 mV, more negative of HNTs. In the nanomaterial HNTs/**2** indeed, PNA molecules interact with the HNTs lumen leading to a partial neutralization of the internal positive charge as demonstrated by the lower ζ-potential value in comparison to pristine HNTs.

The morphology of the different nanomaterials was imaged by TEM and high-angle annular dark field scanning transmission electron microscopy (HAADF-STEM). The TEM images of all HNTs/PNA nanomaterials (Figures 6a-c and S.1) showed the characteristic tubular structure of halloysite. Energy-dispersive X-ray spectroscopy (EDS) elemental mapping showed that the PNA molecules were present on the overall surface of the tubes, as highlighted by the distribution of N atoms (highlighted in red in all samples). Moreover, close observation of the tubes showed the presence of N atoms localized in different portions of the tubes depending on the PNA tetramer loaded into HNTs. In particular, EDS elemental mapping performed along the HNTs section highlighted the presence of N atoms at the external surface in the case of nanomaterial HNTs/**1** (Figure 6a), in the lumen in the case of HNTs/**2** (Figure 6b) and colocalized at both surface in HNTs/**3** (Figure 6c) confirming the aforementioned hypotheses. It should be also noted that in the case of the nanomaterial HNTs/**3** (Figure 6c) the external surface of HNTs appears to be less defined probably due to low contrast of C atoms due to their low atomic number Z, further confirming the presence of organic matter interacting with it.

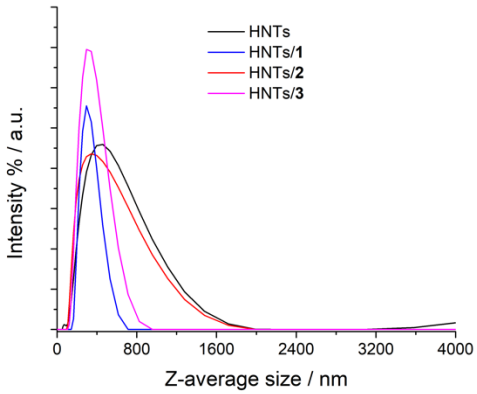

Figure 5. Distribution functions of Z-average size value of HNTs, HNTs/**1**, HNTs/**2** and HNTs/**3** nanomaterials.

Table 1. Average size, polydispersity index and ζ-potential values for HNTs, HNTs/**1**, HNTs/**2** and HNTs/**3** nanomaterials. Reported are the mean ± SD values of three independent experiments run in triplicate.

Nanomaterial	Z-average size (nm)	PDI	ζ-potential value (mV)
HNTs	422 ± 30	0.31 ± 0.04	–34
HNTs/**1**	329 ± 10	0.23 ± 0.01	–31.9
HNTs/**2**	484 ± 16	0.43 ± 0.04	–39
HNTs/**3**	320 ± 10	0.25 ± 0.03	–30.9

Kinetic release

To evaluate the performances of the obtained nanomaterials for application in biomedical field, the kinetic release of the different PNA tetramers from HNTs/**1**, HNTs/**2** and HNTs/**3** nanomaterials was evaluated by the dialysis bag method at pH 7.0 and pH 3.0 to mimic physiological conditions. In particular pH 3.0 was chosen to simulate gastric pH for potential oral administration of the obtained nanomaterials. The obtained kinetic data are reported in Figure 7. As it is possible to observe, the release of PNA tetramer **1** from HNTs/**1** nanomaterial was very fast reaching the 100 wt% of molecules released after ca. 300 min at both pH investigated (Figure 7a). This behavior agrees with the desorption of molecules from the HNTs external surfaces.

Regarding the release of **2** from the HNTs/**2** nanomaterial, it showed different behavior depending to the release medium. In particular, it was observed that, in acidic medium, the total amount of **2** loaded into HNTs was released from the carrier in ca. 350 min, while a slow release at pH 7.0 was observed, and in this case the total amount of PNA loaded was released after 24 h. These findings could be explained by the existence of electrostatic attraction interactions existing between the negative charged tetramer **2** and the positively charged HNTs lumen, that are missing at pH 3.0. The HNTs/**3** nanomaterial showed a different behavior. In this case both at pH 3.0 and pH 7.0 a slow release of the tetramer **3** was observed, where ca. 40 wt% of the total tetramer loaded is released after 500 min, reaching a plateau after 24 h (Figure 7b).

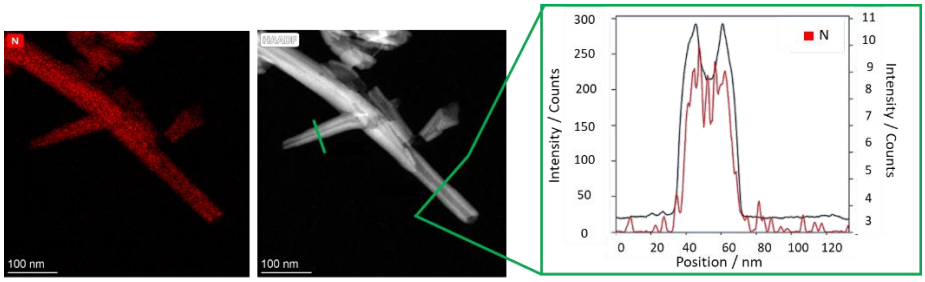

(a)

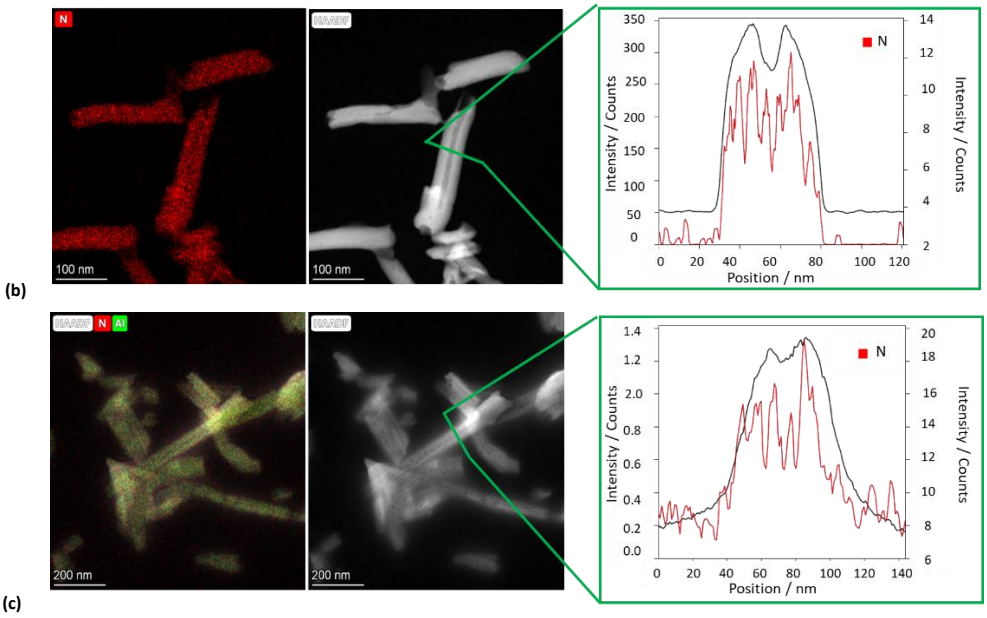

Figure 6. TEM, HAADF-STEM images EDS elemental mapping of N atoms along the selected area of the HAADF-STEM image of (a) HNTs/**1**, (b) HNTs/**2** and (c) HNTs/**3** nanomaterials.

This is in agreement with the presence of **3** at both HNTs surfaces, indeed, it was possible to hypothesize that could exist some attraction interactions between the PNA molecules which slow down the overall release as observed for other kind of molecules released by the tubes.[22]

Similar results were found by Bertucci *et al.* who reported that by tuning the net charge of specific PNA loaded into porous silicon nanoparticles it is possible to modulate the temporal profile of the delivery process.[23]

The kinetic data were analyzed by different mathematical models to obtain information about the release mode. In particular different models, namely zero-order, first-order, Power Fit and the combination of two different models, namely zero and first order model, were applied. The obtained fits revealed that the release of **1** from HNTs/**1** follows the first order at both pH model ($k = 0.021 \pm 0.002$ min^{-1}, $R^2 = 0.9899$ and $k = 0.043 \pm 0.003$ min^{-1}, $R^2 = 0.9967$ at pH 3.0 and 7.0, respectively) indicating a fast desorption from the HNTs external surface. On the contrary, the release of **2** is better explained by the sum of an exponential and a linear term ($k_1 = 0.05 \pm 0.01$ min^{-1}, $k_2 = 0.048 \pm 0.004$ min^{-1}, $R^2 = 0.9852$) at pH 3.0, due to the diffusion of **2** from the lumen which could probably interact with the HNTs external surface by hydrogen bonding interaction and thus fast released in the medium. Conversely, in neutral conditions, the experimental data are well fitted by a first order model ($k = 0.017 \pm 0.003$ min^{-1}, $R^2 = 0.9846$) indicating a slow diffusion from the HNTs lumen.

Regarding PNA **3**, its release from the HNTs/**3** nanomaterial at pH 3.0 is better described by a first order model ($k = 0.008 \pm 0.001$ min^{-1}, $R^2 = 0.9748$) in agreement with a diffusion/desorption from HNTs surfaces.

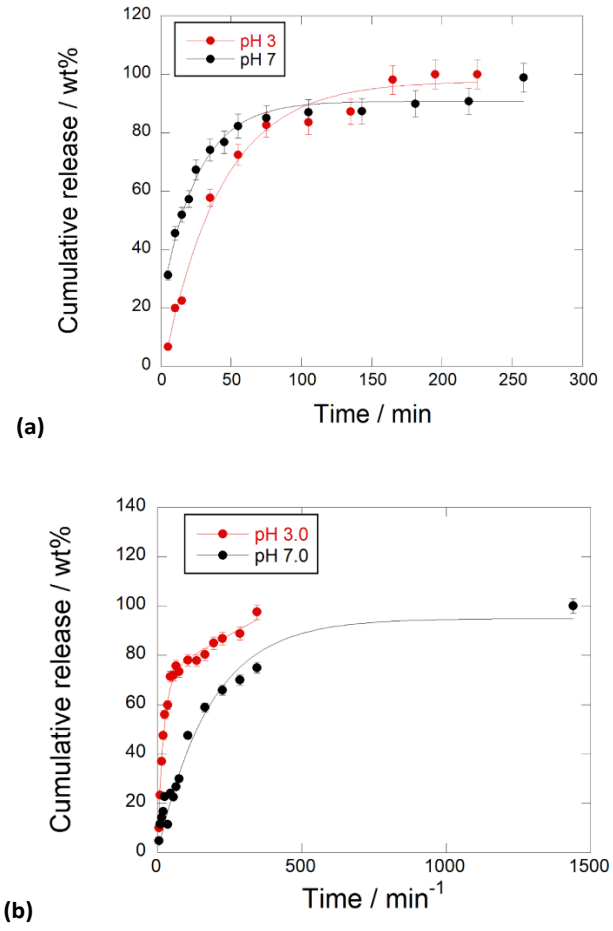

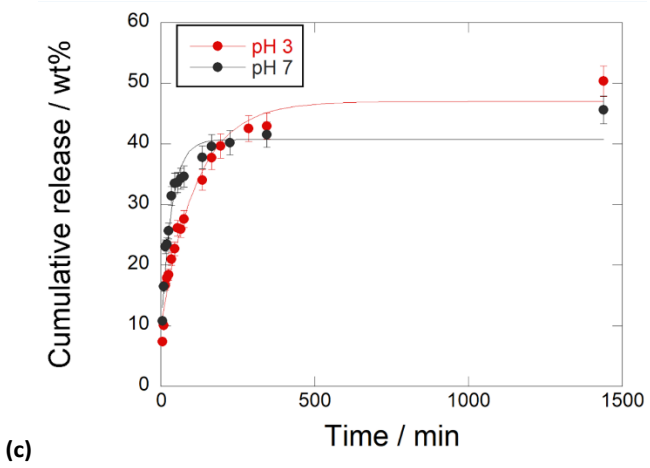

Figure 7. Kinetic release of PNA tetramers from (a) HNTs/**1**, (b) HNTs/**2** and (c) HNTs/**3** nanomaterials at pH 3.0 and pH 7.0, 37 °C. Reported are the mean ± standard deviation values.

Conversely, at pH 7.0, the kinetic data are better fitted by the sum of an exponential and a linear term (k_1 = 0.051 ± 0.004 min^{-1}, k_2 = 0.005 ± 0.001 min^{-1}, R^2 = 0.9748). The latter results could agree with the interaction of **3** with both HNTs surface.

Molecular modelling

PNA tetramers

The tetramer structures optimized with COMPASS force field (FF) have most of the heterocycle rings of nucleobase in a parallel disposition each other, except the adenine one. The relative conformation of the nucleobase rings was similar in all cases. Intramolecular interactions are responsible of this conformation. The heterocyclic rings are at 2.90-3.90 Å each other, then π-π interactions can be considered. Besides, carbonyl O atoms interact with alkyl H atoms with d(CO…HC) = 2.57-3.25 Å including the polypeptide amide carbonyl groups. This polypeptide chain can facilitate this relative parallel disposition of nucleobases.

On the other hand, the tetramer structures optimized with DMol[3] in an aqueous environment have all heterocyclic rings in a parallel orientation each other, except the adenine ring in the chloride salt of PNA **2** (Figure 8).

The average distance between heterocyclic rings is 2.4-3.0 Å owing to π-π interactions and some hydrogen bonds C=O…HC. The peptidic chain is maintained by hydrogen bonds between carbonyl groups and NH and CH groups, d(CO…HN) = 1.915-2.600 Å, d(CO…HC) = 2.39-3.03 Å. This orientation is similar to that observed experimentally in the crystal structure of a peptide nucleic acid duplex from X-ray diffraction,[24] where there is an aqueous environment with the crystallization water molecules. Hence, the presence of water molecules facilitates the co-planarity of all nucleotide rings in these tetramers.

For confirming the validation of these calculations, the IR frequencies of the main vibrational modes were calculated and compared with the values of the experimental spectra (Table 2).

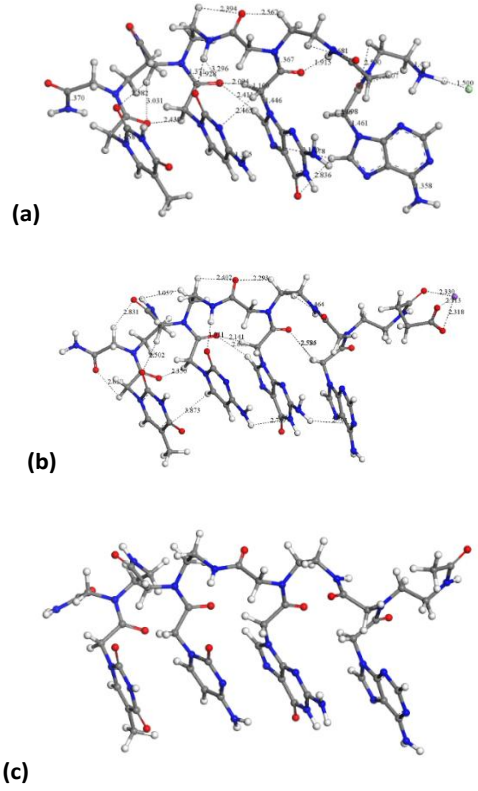

Figure 8. Molecular structures optimized by DFT in aqueous media PNA tetramer **1** (chloride salt) (a), PNA tetramer **2** (Na salt) (b), and PNA tetramer **3** (c). The main intramolecular interactions are described by dashed lines. The H, C, N, and O atoms are in white, gray, blue and red colors, respectively. This criterium is applied to the rest of atomic models in this work.

Table 2. Frequency (in cm^{-1}) of the main vibrational modes calculated by DMol[3] for the PNA structures.

Mode	PNA tetramer 1	PNA tetramer 2	PNA tetramer 3
$\nu(NH_2)_{as}$	3650[a], 3644[b], 3639[c], 3598[d]	364c[g], 3641[a], 3639[b], 3585[d], 3529[e]	3661[c], 3648[b], 3644[a], 3585[d]
$\nu(NH_2)_s$	3518[a], 3506[b], 3504[c], 3494[d]	3511[a,c], 3499[b], 3480[d]	3527[c], 3513[a], 3505[b]
ν(NH)	3524[e], 3507[f], 3498[a], 3468[g], 3348-3344[e], 3173[g]	3517[f], 3509[d], 3496-3462[e], 3330[e]	3518[b], 3516[f], 3508[d], 3482-3320[e]
ν(CH)	3227[c], 3221[c], 3211-3194[a], 3188[f], 3153[b], 3117[c]	3268[c], 3218[d], 3215[a],3206[f], 3181[a], 3150[c]	3222[c], 3220[f], 3219[a,d], 3157[a], 3127[c]
$\nu(CH_2)$	3144-3024	3149-3071, 3054-2993_s	3165-3158, 3148-3138, 3126-2989
$\nu(CH_3)$	3079, 3018-3005_s[f]	3126, 3012_s	3107, 3000_s[f]
ν(C=O)	1764[d], 1749[b], 1738[e], 1735[f], 1727[e], 1725[f], 1708-1678[e]	1746[d], 1742[b], 1718[f], 1711[b], 1706[f], 1698-1655[b], 1646[b], 1551[h]	1757[d], 1735[b], 1709[e], 1707[b], 1706[f], 1705[e], 1697[f], 1673-1646[e]
Ring	1573[c], 1566-1518[d], 1509-1480[a]	1651[a,f], 1580[c], 1576-1552[d], 1513[a], 1480[c]	1667[f], 1650[a], 1580[c]
$\delta(NH_2)_s$	1633[d,g], 1629[e], 1623[c], 1584[a], 1553[b]	1639-1589, 1565-1654	1630-1560
δ(NH)	1542-1533[b], 1451, 1385-1310	1525-1520, 1495, 1451, 1380-1376	1526-1521
δ(CH)	1676[f], 1649[a], 1489-1483[c], 1486-1454[e], 1446-1403_s[e]	1475-1452, 1449-1399, 1381	1475-1405
ν(C-NH_2)		1488	
$\delta(CH_3)$	1457[f]	1436, 1394_s	
γ(CH)	1385-1310, 880-758	1374-1316, 1312-1180, 1165-774, 697-640	1235-1209[e], 775[d]
γ(NH)	961-926[g], 720-667[e]	760[f], 744[d], 705[f]	739-684_s

[a] Cytosine. [b] Chain terminal amide group. [c] Adenine. [d] Guanine. [e] Peptidic chain. [f] Thymine. [g] Ammonium cation. [h] Carboxylate.

The calculated frequencies are consistent with the experimental spectra in all cases. The broad multiple band that appears at 3650-2900 cm^{-1} in the experimental spectra corresponds to the overlapping result of the stretching modes of NH and CH bonds. The bands at higher than 3300 cm^{-1} frequencies are assigned to the stretching vibration modes of N-H bonds. The shoulder observed at frequencies higher than 3520 cm^{-1} in the experimental spectra can be assigned to the asymmetric stretching mode of the NH_2 group, $\nu(NH_2)_{as}$. Our calculations allow distinguishing the vibration modes of different amino groups, from adenine, cytosine, guanine, the terminal amide, and those from the peptidic chain. The $\nu(NH_2)_{as}$ mode of adenine shows higher frequency in **2** and **3**, except in **1** due to the different torsional position of the heterocyclic ring. On the contrary, guanine shows the lowest frequencies probably due to the interactions with vicinal heterocycles. A similar effect is observed in the symmetric mode of $\nu(NH_2)_s$ whose bands appear at slightly lower frequencies and they can be within the high-frequency shoulder of the experimental band. The ν(NH) bands of the N-H groups appear at slightly lower frequencies than above ones. The NH groups of the peptide chain show lower frequencies due to intramolecular interactions of vicinal C=O groups. In **1** the ν(NH) mode of the ammonium group appears at lower frequency than other NH groups. The bands that appear at the frequency range 3268-2989 cm^{-1} are assigned to the stretching mode of the C-H bond of the CH, CH_2, and CH_3 groups.

The intense band observed experimentally at 1760-1550 cm^{-1} is the overlapping of bands assigned to the stretching ν(C=O), bending $\delta(NH_2)_s$ and ring deformation modes. The shoulder at higher frequency corresponds to ν(C=O) where small frequency differences between CO groups can be observed in our calculations, owing to different electronic and intramolecular interactions. In **2** the ν(C=O) of carboxylate appears at lower frequency 1551 cm^{-1}. The small band observed experimentally at 1525-1500 cm^{-1} can be assigned to the δ(NH) mode confirmed by our calculations. The bands appearing at the 1480-1350 cm^{-1} range of the experimental spectra are assigned by our calculations to several δ(NH) and δ(CH) modes. The bands at 1100-1230 cm^{-1} of the experimental spectra are assigned to the out-of-plane deformation mode, γ(CH). In **1**, the experimental spectrum shows a band at 930-980 cm^{-1} assigned to γ(NH) of the ammonium group by our calculations, whereas the γ(NH) mode of the rest of groups appears at 850-640 cm^{-1} along with some bands of γ(CH).

The IR spectra of these molecules were simulated (Figure 9) being consistent with the experimental ones (Figure 4a).

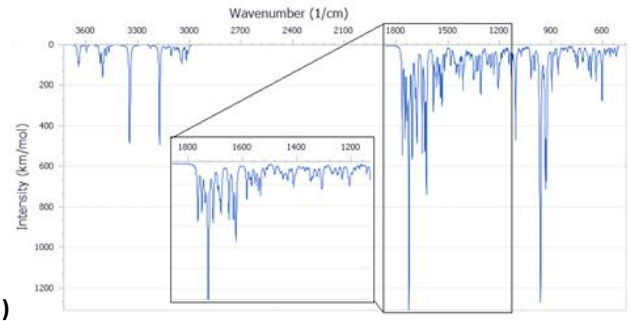

(a)

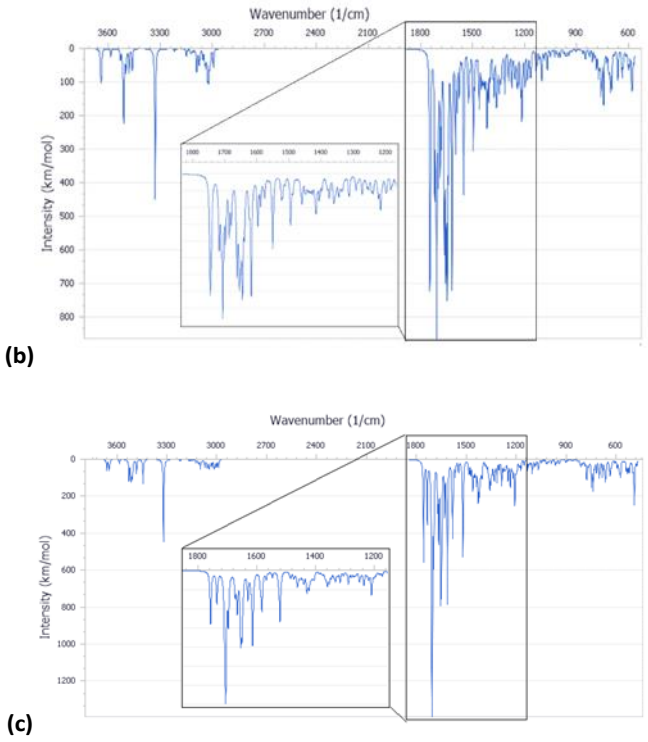

Figure 9. IR spectra simulated from the calculated molecular structure with DFT for PNA tetramer **1** (chloride salt) (a), PNA tetramer **2** (Na salt) (b), and PNA tetramer **3** (c).

PNA tetramers adsorption on the internal or/and external surfaces of the halloysite

Following the experimental data, we studied the adsorption of three tetramers of PNA on the halloysite. Specifically, we generated four models: the halloysite with the tetramer **1** adsorbed on the external surface; the halloysite with the tetramer **2** adsorbed on the internal surface; the halloysite with the tetramer **3** adsorbed on the external surface; and the halloysite with the tetramer **3** inside the nanotube. After the equilibration and optimization of theses complexes with COMPASS force field, the resultant structures were analyzed (Figure 10).

In all the adsorption complexes (Figure 10), the PNA tetramers are positioned with an orientation parallel to the surface of the nanotube with a mainly flat conformation. Moreover, when the PNA tetramers are adsorbed on the external surface of the nanotube, hydrogen bonds interactions between the hydrogen atoms of the tetramers and the oxygen atoms of the surface around 2.5 Å were found. While when the PNA tetramers are adsorbed on the internal surface of the halloysite, the mainly interactions were hydrogen bonds between the oxygen of the carbonyl groups and the hydrogens of the internal surface around 2.0 Å.

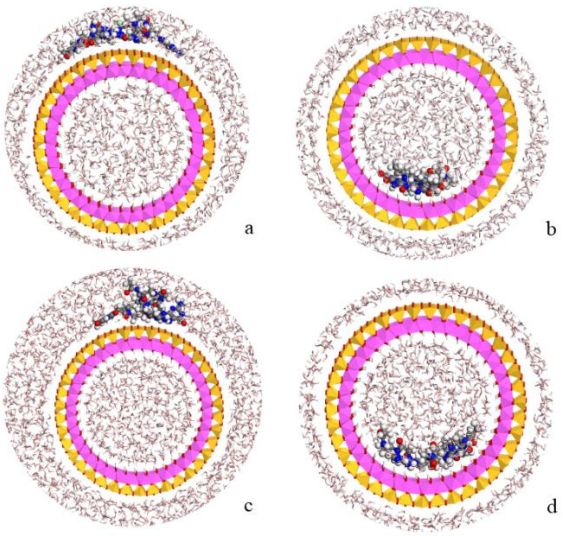

Figure 10. Complexes of the PNA tetramer **1** adsorbed on the external surface of the halloysite (a), of the PNA tetramer **2** adsorbed on the internal surface (b) and of the PNA tetramer **3** adsorbed on the external (c) and internal (d) surfaces of the nanotube in water solution. The atoms of silicon, aluminum, oxygen, hydrogen, carbon, nitrogen, chlorine and sodium are presented in yellow, pink, red, white, grey, blue and slight green and purple, respectively.

Lastly, the adsorption energies of the models were compared according to the equation $E_{ads}= (E_{COMPLEX}) - (E_{PNA} + E_{HNTs})$. The adsorption energy of complex with the PNA tetramer **1** (Figure 10a) was −157.7 kcal/mol, of the complex with the PNA tetramer **2** (Figure 10b) was −222.4 kcal/mol, of the complex with the PNA tetramer **3** adsorbed on the external surface (Figure 10c) was −127.3 kcal/mol and inside the nanotube (Figure 10d) was −51.3 kcal/mol. The results showed that all the complexes presented a negative adsorption energy. Therefore, the loading of the PNA tetramers is favorable on the halloysite nanotube.

Experimental

Materials and methods

All the reagents and solvents were purchased from commercial sources and used without further purification.

Halloysite nanotubes used in this study were obtained from Merck and used as received.

The monomers Boc-PNA-T-OH (>95%), Boc-PNA-C(Z)–OH (>95%), Boc-PNA-G(Z)–OH (>95%), Boc-PNA-A(Z)–OH (>95%), Fmoc-PNA-T-OH (>95%), Fmoc-PNA-C(Bhoc)-OH (>95%), Fmoc-PNA-G(Bhoc)-OH (>95%), Fmoc-PNA-A(Bhoc)-OH (>95%) were purchased from ASM Research Chemicals GmbH (Hannover, Germany). HNTs (lyophilized powder, MQ200) were purchased from Merck (Darmstadt, Germany). Polystyrene MBHA resin (0.88 mmol/g) was purchased from Novabiochem, and the H-rink amide ChemMatrix® (0.60 mmol/g) was purchased from Merck (Darmstadt, Germany). Polypropylene one-way syringes and the corresponding polytetrafluoroethylene (PTFE) frits, used as reactor for the manual solid phase synthesis, were

purchased from Alltech Associates Inc. (Lokeren, Belgium). The reverse-phase RP-HPLC purification of PNA tetramers **1**-**3** was performed on an Agilent 1200 Series system, using the semi-preparative Luna C18 column (25 cm x 10 nm, 5 μm). A binary mixture of solvents A (water + 0.1% TFA) and B (acetonitrile + 0.1% TFA) was used as mobile phase. Chromatographic purifications were performed at room temperature, with a constant flow rate of 3 mL/min and linear gradients. The absorbance was measured at 260 and 280 nm. UPLC-MS analyses were recorded on an Acquity UPLC I-class instrument (Waters) equipped with Acquity PDA detector (Waters). Chromatographic separation was performed using the column ACQUITY UPLC BEH C18 (100 × 2.1 mm, 1.7 μm) (Waters) fitted with a VanGuard cartridge (Waters) for tetramer **3**, and the column ACQUITY UPLC HSS T3 C18 (100 × 2.1 mm, 1.8 μm) (Waters) fitted with a VanGuard cartridge (Waters) for tetramers **1** and **2** at a constant flow rate of 0.4 mL/min. A binary mixture of solvents A (water + 0.1% formic acid) and B (acetonitrile + 0.1% formic acid) was used as mobile phase. The absorbance was measured at 260 nm. HR-ESI$^+$ MS(/MS) analyses were recorded with Synapt G2-*Si* QToF instrument (Waters) interfaced through a Zspray^{TM} ESI-probe for electrospray ionization (Waters).

The concentration of PNA solutions in aqueous solution was determined by measuring the absorbance at 260 nm with an Agilent 8453 UV/Vis spectrophotometer. The molar extinction coefficient of PNA tetramers was calculated according to literature.[25] Water HPLC Plus grade (Merck) was used to prepare PNA solutions and for the loading experiments of PNAs on HNTs.

Suspension of HNTs in water were sonicated with an Elmasonic S30H sonicated at T = 30 °C. The vacuum/air cycles were performed using a vacuum chamber connected to a diaphragm vacuum pump and a VC-900 vacuum regulator. The FT-IR spectra were registered using a Jasco Mod FT-IR 4600 Infrared spectrometer in transmittance mode. The DLS and Zeta Potential analyses were registered using a Malvern Zetasizer Nano instrument at 25 °C, equipped with a 633 nm solid state He-Ne laser at a scattering angle of 173°. The TGA analyses of were performed by means of a Perkin Elmer TGA thermogravimetric analyser, under air in a temperature range from 30 °C to 800 °C at the heating rate of 10 °C/min.

Transmission Electron Microscopy (TEM) was performed by means of a FEI Titan G2 60–300 ultra high resolution transmission electron microscope coupled with Analytical Electron Microscopy (AEM) performed with a SUPER-X silicon-drift windowless X-ray Energy-Dispersive Spectroscopy (XEDS) detector. AEM spectra were saved in mode STEM (Scanning Transmission Electron Microscopy) with a HAADF (High Angle Annular Dark Field) detector. X-ray chemical element maps were also collected.

Synthetic procedures

Synthesis of tetramer 1 according to Boc/Z strategy.

The MBHA resin (150 mg, 0.3 mmol/g, 0.045 mmol), downloaded with the Boc-PNA-T-OH monomer, was swollen in CH_2Cl_2 for 40 min, and the Boc group of the anchored monomer was removed by the treatment with a mixture of TFA/*m*-cresol (95/5 v/v, 2 × 4 min). The resin was then washed with CH_2Cl_2 and NMP, and finally with a solution of DIPEA in CH_2Cl_2 (5% *w/w*). In a vial, a solution of DIPEA (10 eq, 0.45 mmol, 78 μL) and the Boc/Z protected monomer (5.3 eq, 0.239 mmol) in NMP was added to a solution of HATU (4.8 eq, 0.216 mmol, 82 mg) in NMP, and the resulting mixture was shaken for 2 min. The activated acid was then transferred to the resin and shaken for 2 h at room temperature. The resin was then washed with NMP and CH_2Cl_2. The two-step cycle, Boc-deprotection and coupling, was repeated for each PNA monomer to obtain the resin-supported PNA tetramer **4**. Subsequently, the resin was washed with TFA, and then shaken with a cleavage mixture of TFA/TFMSA/thioanisole/*m*-cresol (6/2/1/1, v/v/v/v) for 1.5 h at room temperature. After filtration and partial evaporation of TFA, the PNA **1** was precipitated in ice-cold diethyl ether, and the precipitate was dried, dissolved in water, and purified by RP-HPLC. Pure PNA fractions were collected and concentrated to dryness using lyophilizer, and PNA sample **1** was obtained as colorless powder. HR-ESI$^+$ MS: m/z found (calculated): 1101.4550 (calc. for $C_{43}H_{57}N_{24}O_{12}$, 1101.4588) $[M+H]^+$, 551.2331 (551.2333) $[M+2H]^{2+}$.

Synthesis of tetramer 1 according to Fmoc/Bhoc strategy.

The ChemMatrix® resin (150 mg, 0.3 mmol/g, 0.045 mmol), downloaded with the Fmoc-PNA-T-OH monomer, was swollen in CH_2Cl_2 for 40 min, and the Fmoc group of the anchored monomer was removed by the treatment with a solution of piperidine in NMP (1:5, v/v, 2 × 8 min). The resin was then washed with CH_2Cl_2 and NMP. In a vial, a solution of DIPEA (10 eq, 0.45 mmol, 78 μL) and the Fmoc/Bhoc protected monomer (5.0 eq, 0.239 mmol) in NMP was added to a solution of HATU (5.0 eq, 0.216 mmol, 82 mg) in NMP, and the resulting mixture was shaken for 2 min. The activated acid was then transferred to the resin and shaken for 2 h at room temperature. The resin was then washed with NMP and CH_2Cl_2. The two-step cycle, Boc-deprotection and coupling, was repeated for each PNA monomer to obtain the resin-supported PNA tetramer **5**. The resin was treated with a solution of piperidine in NMP (1:5, v/v, 2 × 8 min), and then washed with NMP and CH_2Cl_2. Subsequently, the resin was dried under vacuum and treated with a cleavage mixture of TFA/*m*-cresol (9/1, v/v) for 1.5 h at room temperature. After filtration and partial evaporation of TFA, the PNA **1** was precipitated in ice-cold diethyl ether, and the precipitate was dried, dissolved in water, and purified by RP-HPLC. PNA sample **1** was isolated in similar amount and purity than those obtained following the Boc/Z strategy.

Synthesis of tetramer 2.

The resin-supported PNA tetramer **4** (150 mg, 0.3 mmol/g, 0.045 mmol) was swollen in CH_2Cl_2 for 40 min, and the Boc group of the anchored monomer was removed by the treatment with a mixture of TFA/*m*-cresol (95/5 v/v, 2 × 4 min). The resin was washed with CH_2Cl_2, treated with a solution of DIPEA in CH_2Cl_2 (5% *w/w*, 2 × 4 min), and then washed with DCM and NMP. A solution of succinic anhydride (20 eq, 0.9 mmol, 90 mg) in NMP was transferred to the resin and shaken for 4 h at

room temperature. The resin was then washed with NMP and CH_2Cl_2 and the protocol for the cleavage according to Boc/Z strategy provided the crude PNA **2**, which was purified by RP-HPLC. HR-ESI$^+$ MS: m/z found (calculated): 1201.4734 (calc. for $C_{47}H_{61}N_{24}O_{15}$, 1201.4748) $[M+H]^+$, 601.2408 (601.2413) $[M+2H]^{2+}$.

Synthesis of tetramer 3.

The resin-supported PNA tetramer **4** (150 mg, 0.3 mmol/g, 0.045 mmol) was swollen in CH_2Cl_2 for 40 min, and the Boc group of the anchored monomer was removed by the treatment with a mixture of TFA/*m*-cresol (95/5 v/v, 2 × 4 min). The resin was washed with CH_2Cl_2, treated with a solution of DIPEA in CH_2Cl_2 (5% *w/w*, 2 × 4 min), and then washed with DCM and NMP. A solution of acetic anhydride (20 eq, 0.9 mmol, 85 μL) in NMP was transferred to the resin and shaken for 4 h at room temperature. The resin was then washed with NMP and CH_2Cl_2 and the protocol for the cleavage according to Boc/Z strategy provided the crude PNA **3**, which was purified by RP-HPLC. HR-ESI$^+$ MS: m/z found (calculated): 1143.4698 (calc. for $C_{45}H_{59}N_{24}O_{13}$, 1143.4693) $[M+H]^+$, 572.2385 (572.2386) $[M+2H]^{2+}$.

General procedure for the loading of PNA tetramers 1–3 on HNTs.

To a dispersion of pristine HNTs (50 mg) in H_2O (2.5 mL), 0.500 mL of a solution 10 mM of **1–3** in H_2O were added. The obtained dispersion was evacuated for 30 min at 200 Torr, left to stir at atmospheric pressure for 15 min, and this cycle was repeated twice. Finally, the dispersions were stirred at room temperature for 16 h. After this time, the dispersions were centrifuged and the obtained powders were washed with water, and then lyophilized to dryness.

Kinetic release

The release of the three PNA tetramers from HNTs/PNA nanomaterials was done as follows: 15 mg of the sample were dispersed in 1 mL of dissolution medium (HCl 1×10^{-3} N and phosphate buffers at pH 3.0 and 7.4, respectively) and transferred into a sealed dialysis membrane (Medicell International Ltd MWCO 12–14000 with a diameter of 21.5 mm). Subsequently the membrane was put in a round bottom flask containing 9 mL of the release medium at 37 °C and stirred. At fixed time, 1 mL of the release medium was withdrawn and analyzed by UV–vis measurements at λ of 260 nm. To ensure sink conditions, 1 mL of fresh solution was used to replace the collected one. Total amounts of drug released (F_t) were calculated as follows:

$$F_t = V_m C_t + \sum_{i=0}^{t-1} V_a C_i \qquad (Eq.1)$$

where V_m and C_t are the volume and the concentration of PNA tetramer at time *t*. V_a is the volume of the sample withdrawn and C_i is the PNA tetramer concentration at time *i* ($i < t$).

Models

The PNA tetramers **1**–**3** models were generated sketching by hand by using the Materials Studio package[26] taking into account the experimental information. The terminal amino group of PNA tetramer **1** was protonated and neutralized with a chloride anion according to experimental conditions. Analogously, the carboxylate terminal group of PNA tetramer **2** was neutralized with a Na^+ cation following the experimental conditions. A zwitterionic form of a neutral PNA tetramer **3** model was also generated and inserted in a periodical box of 15×15×35 Å along with 226 water molecules filled by Monte Carlo method reaching a final density of 1 g/cm^3. In the same way, the water molecule was previously generated by hand.

On the other hand, a slide of halloysite nanotube, with the stoichiometry $Al_2Si_2O_5(OH)_4$, was obtained from a previous work.[27] Subsequently, a periodical crystal structure of this nanotube was generated using periodic boundary conditions [22, 28, 29] The unit cell of halloysite has the formula $Al_{76}Si_{76}O_{190}(OH)_{152}$ with 646 atoms, and an internal diameter of 27 Å. This structure is a proper model to study the drug-clay adsorption process. To carry out the adsorption of PNA tetramer, a 1×1×4 supercell of halloysite was generated with the formula $Al_{304}Si_{304}O_{760}(OH)_{608}$ and with 2584 atoms.

Molecular modeling methodology

The geometry optimization of PNA tetramers **1**–**3** were performed with the COMPASS force field[30] based on empirical interatomic potentials and using the Forcite code.[26] The water molecule was also optimized with the COMPASS force field. Additionally, the solvation free energy of PNA tetramer **3** was calculated by means of molecular dynamics simulations of the periodical box with the zwitterionic model of the neutral PNA tetramer **3** and water molecules. After a simulation with the NVE ensemble with 1 fs steps during 5 ps, an additional simulation was performed at NVT ensemble during 50 ps. Moreover, quantum mechanical calculations based on Density Functional Theory (DFT) were performed by using the DMol^3 code[31] with GGA and PBE[26] functionals. Double numerical plus polarization functions was used for the atomic orbital basis sets with a cut-off of 3.5 Å. The Grimme semiempirical dispersion correction was used[32] and DFT semi-core pseudopotentials (DSPP)[33] were applied. The COSMO (COnductor like Screening MOdel) approach[34] was used for simulating a solvent environment of an aqueous media (dielectric constant = 78.54). The IR frequencies of the main normal vibration modes were calculated analyzing the Hessian matrix produced by finite atomic displacements.

On the other hand, the optimization of the unit cell of halloysite nanotube structure was performed with quantum mechanical calculations by using DFT with CASTEP code.[26] The functionals used were GGA and PBE. On-the-fly generated (OTFG) ultrasoft pseudopotentials were used with Koelling-Harmon relativistic treatment,[35] and the cut off energy of the calculation was 300 eV.[26] After the optimization of the halloysite unit cell, the 1×1×4 supercell was created to study the adsorption of the PNA tetramers and this halloysite structure was fixed, except the hydrogen atoms of the internal surface.

The PNA tetramers **1–3** were placed on the internal and/or external surface of the halloysite, following the experimental data. Four complexes were prepared: the halloysite with the tetramer **1** adsorbed on the external surface; the halloysite with the tetramer **2** adsorbed on the internal surface; the halloysite with the tetramer **3** adsorbed on the external surface; and the halloysite with the tetramer **3** inside the nanotube. These drug-halloysite complexes were optimized and, subsequently, 100 ps of NVT molecular dynamic simulation was performed to equilibrate the systems using Forcite with COMPASS.[26] Later, the last structure of the dynamics was again optimized and filled with the previously optimized water molecules using Monte Carlo method with COMPASS.[26] In this way, the water with a density of 1 g/cm^3 filled the adsorption complexes (~ 3444 water molecules). After that, the resultant adsorption complexes were optimized with COMPASS to obtain the most stable structure and calculate its energy.

The adsorption energy of the complexes was estimated using the equation $E_{ads} = (E_{COMPLEX}) - (E_{PNA} + E_{HNTs})$. For this, the energy of the optimized adsorption complexes was calculated ($E_{COMPLEX}$), as well as the tetramers and the halloysite with the water of the optimized complexes were isolated and the optimized energy were calculated (E_{PNA} and E_{HNTs}), with the COMPASS force field.[26]

Conclusions

Halloysite is a versatile nanomaterial which has shown promising features for application in nanomedicine. Because of its peculiar structure, different surface charges and the presence of an empty lumen, it is efficiently used as nanocontainer for the delivery of active species.

In the present work, the supramolecular interaction of the clay with three differently charged PNA tetramers, chosen as models, was carried out.

Firstly, the PNA tetramers **1**–**3** were prepared manually according to standard protocols for solid-phase synthesis of PNAs by adopting two different procedures, namely the Boc/Z and Fmoc/Bhoc strategies, depending on the charge that would introduced onto them.

Afterwards, they were loaded onto halloysite by following a standard procedure adopted for the supramolecular loading of organic molecules onto HNTs.

The obtained nanomaterials were characterized by FT-IR spectroscopy and thermogravimetric analyses that allowed to calculate the loading percent of each PNA into HNTs. DLS and z-potential measurements highlighted that the three different nanomaterials possess different aqueous diffusion features and different surface charges in agreement with the different HNTs surface interacting with the PNA tetramers. Indeed, the interaction of negatively charged PNA **2** with HNTs led to the synthesis of a nanomaterial with similar Z-average size of HNTs and more negative surface charge in agreement with its lumen confinement. On the contrary, the interaction of halloysite with the positively charged PNA and the neutral one did not lead to any variation in the charge of the nanomaterials in comparison to HNTs, but they showed a slight increase in the average size of the nanomaterials. These findings were explained by considering the interaction of the positively charged PNA **1** with the HNTs external surface and that of neutral **3** with both surfaces.

Morphological characterizations by HAADF/STEM investigations highlighted the presence of the PNA tetramers at the external or inner surface or on both depending on their charge, as proved by the EDS elemental mapping along tube section. Kinetic release experiments at different pH mimicking physiological conditions showed that PNA **3** is slowly released over the time, whereas the release of PNA **1** and **2** is ruled by electrostatic forces.

Lastly, theoretical calculations were performed to study the structures of the tetramers and to obtain the IR spectra of these molecules, being consistent with the experimental ones. Furthermore, the simulations confirmed the adsorption of the tetramers on the halloysite, showing hydrogen bonds and electrostatic interactions taking place between the tetramers and the internal and/or external surfaces of the HNTs. The favorable adsorption processes observed in the experimental results were also confirmed.

In summary, this study reports the possibility to combine the PNA features with a low cost, naturally available in large amounts and biocompatible carrier as halloysite. Furthermore, by the supramolecular approach it is possible to scale up the synthesis of these nanomaterials for future potential clinical applications of PNA based systems. The present study opens the doorway for the design of diversified PNA molecules with specific sequences able to interact with halloysite surfaces for the treatment of different pathologies.

Conflicts of interest

"There are no conflicts to declare".

Acknowledgements

Mass spectrometry analyses of PNA tetramers were performed at the Mass Spectrometry facility of the Unitech COSPECT at the University of Milan (Italy). The authors are thankful to Dr. Emma Lambert.

Notes and references

1. S. Pawłowska, T. A. Kowalewski and F. Pierini, *Soft Matter*, 2018, **14**, 8421-8444.
2. M. I. Carretero, *Appl. Clay Sci.*, 2002, **21**, 155-163.
3. D. Peixoto, I. Pereira, M. Pereira-Silva, F. Veiga, M. R. Hamblin, Y. Lvov, M. Liu and A. C. Paiva-Santos, *Coord. Chem. Rev.*, 2021, **440**, 213956.
4. A. Stavitskaya, M. Rubtsova, A. Glotov, V. Vinokurov, A. Vutolkina, R. Fakhrullin and Y. Lvov, *Nanoscale Adv.*, 2022, **4**, 2823-2835.
5. M. Massaro, R. Noto and S. Riela, *Molecules*, 2020, **25**.

6. M. Massaro, S. Pieraccini, S. Guernelli, M. L. Dindo, S. Francati, L. F. Liotta, G. C. Colletti, S. Masiero and S. Riela, *Appl. Clay Sci.*, 2022, **230**, 106719.
7. M. Massaro, M. Notarbartolo, F. M. Raymo, G. Cavallaro, G. Lazzara, M. M. A. Mazza, C. Viseras-Iborra and S. Riela, *ACS Appl. Nano Mater.*, 2022, **5**, 13729-13736.
8. J. Tully, R. Yendluri and Y. Lvov, *Biomacromolecules*, 2016, **17**, 615-621.
9. A. C. Santos, C. Ferreira, F. Veiga, A. J. Ribeiro, A. Panchal, Y. Lvov and A. Agarwal, *Adv. Colloid Interface Sci.*, 2018, **257**, 58-70.
10. M. V. Gorbachevskii, A. V. Stavitskaya, A. A. Novikov, R. F. Fakhrullin, E. V. Rozhina, E. A. Naumenko and V. A. Vinokurov, *Appl. Clay Sci.*, 2021, **207**, 106106.
11. F. R. Ahmed, M. H. Shoaib, M. Azhar, S. H. Um, R. I. Yousuf, S. Hashmi and A. Dar, *Colloids Surf. B*, 2015, **135**, 50-55.
12. E. Rozhina, A. Panchal, F. Akhatova, Y. Lvov and R. Fakhrullin, *Appl. Clay Sci.*, 2020, **185**, 105371.
13. A. Stavitskaya, G. Fakhrullina, L. Nigamatzyanova, E. Sitmukhanova, E. Khusnetdenova, R. Fakhrullin and V. Vinokurov, *Materials*, 2021, **14**.
14. S. Volpi, U. Cancelli, M. Neri and R. Corradini, *Pharmaceuticals*, 2021, **14**, 14.
15. M. Terracciano, F. Fontana, A. P. Falanga, S. D'Errico, G. Torrieri, F. Greco, C. Tramontano, I. Rea, G. Piccialli, L. De Stefano, G. Oliviero, H. A. Santos and N. Borbone, *Small*, 2022, **18**, 2204732.
16. R. Brazil, *ACS Centr. Sci.*, 2023, **9**, 3-6.
17. M. Massaro, E. Licandro, S. Cauteruccio, G. Lazzara, L. F. Liotta, M. Notarbartolo, F. M. Raymo, R. Sánchez-Espejo, C. Viseras-Iborra and S. Riela, *J. Colloid Interface Sci.*, 2022, **620**, 221-233.
18. P. E. Nielsen, *Peptide Nucleic Acids: Methods and Protocols (Third Edition)*, Springer Science + Business Media, LLC, part of Springer Nature 2020, Humana New York, NY.
19. M. Massaro, G. Barone, V. Barra, P. Cancemi, A. Di Leonardo, G. Grossi, F. Lo Celso, S. Schenone, C. Viseras Iborra and S. Riela, *Int. J. Pharm.*, 2021, **599**, 120281.
20. L. Lisuzzo, G. Cavallaro, P. Pasbakhsh, S. Milioto and G. Lazzara, *J. Colloid Interface Sci.*, 2019, **547**, 361-369.
21. L. Lisuzzo, G. Cavallaro, S. Milioto and G. Lazzara, *Polymers*, 2020, **12**, 1766.
22. M. Massaro, A. Borrego-Sánchez, R. Sánchez-Espejo, C. Viseras Iborra, G. Cavallaro, F. García-Villén, S. Guernelli, G. Lazzara, D. Miele, C. I. Sainz-Díaz, G. Sandri and S. Riela, *Appl. Clay Sci.*, 2021, **215**, 106310.
23. M. Neri, J. Kang, J. M. Zuidema, J. Gasparello, A. Finotti, R. Gambari, M. J. Sailor, A. Bertucci and R. Corradini, *ACS Biomaterials Science & Engineering*, 2022, **8**, 4123-4131.
24. H. Rasmussen, J. S. Kastrup, J. N. Nielsen, J. M. Nielsen and P. E. Nielsen, *Nat. Struct. Biol.*, 1997, **4**, 98-101.
25. *https://www.pnabio.com/pdf/PNA_oligomer_handling_PNA Bio.pdf*.
26. M. S. Biovia, Version 2018; Biovia: San Diego, CA, USA, *Journal*, 2018.
27. A. Borrego-Sánchez, C. I. Sainz-Díaz, L. Perioli and C. Viseras, *Molecules*, 2021, **26**, 4392.
28. A. Borrego-Sánchez, A. Hernández-Laguna and C. I. Sainz-Díaz, *J. Mol. Model.*, 2017, **23**, 106.
29. C. Valentino, T. Martínez Rodríguez, A. Borrego-Sánchez, P. Hernández Benavides, F. Arrebola Vargas, J. M. Paredes, S. Rossi, C. I. Sainz Díaz, G. Sandri, P. Grisoli, M. d. M. Medina Pérez and C. Aguzzi, *Pharmaceutics*, 2023, **15**, 1140.
30. H. Sun, *J. Phys. Chem. B*, 1998, **102**, 7338-7364.
31. B. Delley, *The Journal of Chemical Physics*, 2000, **113**, 7756-7764.
32. E. R. McNellis, J. Meyer and K. Reuter, *Phys. Rev. B*, 2009, **80**, 205414.
33. B. Delley, *Phys. Rev. B*, 2002, **66**, 155125.
34. B. Delley, *Molecular Simulation*, 2006, **32**, 117-123.
35. D. Vanderbilt, *Phys. Rev. B*, 1990, **41**, 7892-7895.